



Automatic Detection and Classification of Radio Galaxy Images by Deep Learning

Zhen Zhang¹ , Bin Jiang^{1,3}, and Yanxia Zhang^{2,3}

¹ School of Mechanical, Electrical & Information Engineering, Shandong University, Weihai, 264209, Shandong, People's Republic of China; jiangbin@sdu.edu.cn

² CAS Key Laboratory of Optical Astronomy, National Astronomical Observatories, Beijing, 100101, People's Republic of China; zyx@bao.ac.cn

Received 2021 December 6; accepted 2022 April 14; published 2022 June 29

Abstract

Surveys conducted by radio astronomy observatories, such as SKA, MeerKAT, Very Large Array, and ASKAP, have generated massive astronomical images containing radio galaxies (RGs). This generation of massive RG images has imposed strict requirements on the detection and classification of RGs and makes manual classification and detection increasingly difficult, even impossible. Rapid classification and detection of images of different types of RGs help astronomers make full use of the observed astronomical image data for further processing and analysis. The classification of FRI and FRII is relatively easy, and there are more studies and literature on them at present, but FR0 and FRI are similar, so it is difficult to distinguish them. It poses a greater challenge to image processing. At present, deep learning has made breakthrough progress in the field of image analysis and processing and has preliminary applications in astronomical data processing. Compared with classification algorithms that can only classify galaxies, object detection algorithms that can locate and classify RGs simultaneously are preferred. In target detection algorithms, YOLOv5 has outstanding advantages in the classification and positioning of small targets. Therefore, we propose a deep-learning method based on an improved YOLOv5 object detection model that makes full use of multisource data, combining FIRST radio with SDSS optical image data, and realizes the automatic detection of FR0, FRI, and FRII RGs. The innovation of our work is that on the basis of the original YOLOv5 object detection model, we introduce the SE Net attention mechanism, increase the number of preset anchors, adjust the network structure of the feature pyramid, and modify the network structure, thereby allowing our model to demonstrate galaxy classification and position detection effects. Our improved model produces satisfactory results, as evidenced by experiments. Overall, the mean average precision (mAP@0.5) of our improved model on the test set reaches 89.4%, which can determine the position (R.A. and decl.) and automatically detect and classify FR0s, FRIs, and FRIIs. Our work contributes to astronomy because it allows astronomers to locate FR0, FRI, and FRII galaxies in a relatively short time and can be further combined with other astronomically generated data to study the properties of these galaxies. The target detection model can also help astronomers find FR0s, FRIs, and FRIIs in future surveys and build a large-scale star RG catalog. Moreover, our work is also useful for the detection of other types of galaxies.

Unified Astronomy Thesaurus concepts: [Surveys \(1671\)](#); [Astronomy data analysis \(1858\)](#); [Radio galaxies \(1343\)](#)

1. Introduction

With the emergence and development of large-scale astronomical radio sky survey telescopes in recent years, many radio astronomy observatories, such as the Very Large Array (VLA), ASKAP (Johnston et al. 2008), MeerKAT (Jonas & Team MeerKAT 2016), and SKA (Bourke et al. 2015), have been established. The field of astronomical observation is advancing steadily. The study of the morphology of radio galaxies (RGs) can help us comprehend their formation and evolution and those of their subcomponents as a function of environment, luminosity, star formation rate, and stellar mass over cosmic time (Helfand et al. 2015). The detection and

classification of the massive astronomical RG images obtained by large-scale astronomical radio telescopes are important steps in the study of RG morphology, which is essential for making full use of the astronomical data obtained from observations. Traditional approaches for searching for FR0, FRI, and FRII galaxies require various steps, such as source selection, brightness calculation, and comparison data screening. Several of these steps are prone to failure, require manual intervention, and cannot easily perform an automated batch search in massive image data. Considering the limitations in the efficiency and accuracy of manual classification while faced with massive observation data (Aniyan & Thorat 2017), we developed automatic detection classifiers for FR0, FRI, and FRII RGs based on a deep-learning target detection algorithm.

³ Authors to whom any correspondence should be addressed.

The deep neural network model built by the target detection algorithm can automatically locate the RG of interest in the image after learning from FR0, FRI, and FRII RG images and can capture small differences between galaxies in images with different types of RGs, thereby realizing the detection and classification of RGs.

RGs include compact and extended types. FR0 belongs to compact RGs, and extended RGs are divided into FRIs and FRIIs according to the Fanaroff–Riley (FR) scheme (Fanaroff & Riley 1974). FR0 and FRI/II represent two extreme examples of radio size and luminosities (Baldi et al. 2018). Most RGs are extended sources and belong to the FRI or FRII category (Fanaroff & Riley 1974; Baldi et al. 2018). These compact sources should be classified as FR0 due to the general lack of extended radio structure (Baldi et al. 2015). Low-intensity RGs are a uniform source population (Baldi et al. 2018). According to the information available on their nuclear properties (Baldi et al. 2015), a common jet-launching mechanism is believed to operate in these celestial objects. Nevertheless, in radio behavior in terms of morphologies, luminosities, and sizes, they are significantly different (Baldi et al. 2018).

The characteristics of FR0 are similar to those found in the host of an FRI RG but are approximately 1.6 times smaller on average. Various scenarios can explain their sizes and abundance compared with FRIs (Baldi et al. 2018). The merger history explains the evolution of the hosts and black hole parameters, leading to the difference between FR0 and FRI sources (Baldi et al. 2018). Moreover, the difference between the two categories is not only in size but also in their radio-core dominance and in the ratio between line and radio luminosity, which are both higher in FR0s than in FRIs (Baldi et al. 2018). FR0 is dominated by the core (about 30 times) in comparison with FRIs (Baldi et al. 2015). This condition shows the actual physical difference, which is a diminished capability to generate extended radio radiation.

Extended RGs are classified as FRIs and FRIIs, which have different morphologies (Fanaroff & Riley 1974). The jet and core areas usually have the highest level of surface brightness, so FRIs have a radio morphology with dark edges (Capetti et al. 2017b), whereas FRIIs have a radio morphology with bright edges because FRIIs have remarkable highlighted edges with high surface brightness (Capetti et al. 2017a). Generally, we can distinguish FRIs and FRIIs through different brightness modes in different areas (Alhassan et al. 2018).

The neural network constructed using deep-learning algorithms to classify or detect galaxies has long been applied to various data sources, such as the radio image data in Faint Images of the Radio Sky at Twenty Centimeters (FIRST) (Becker et al. 1995), optical image data in the Sloan Digital Sky Survey (SDSS) (York et al. 2000), and infrared image data in WISE (Jarrett et al. 2011). For example, Alhassan et al. (2018) used FIRST data to classify four types of galaxies by

adopting a classifier based on a deep convolutional network. Maslej-Krešňáková et al. (2021) utilized convolutional neural networks (CNNs) to classify FRI, FRII, BENT, and COMPT galaxies and achieved good results. In addition, redshift estimation (Hoyle 2016), classification of star–galaxy (Kim & Brunner 2017), and prediction of galaxy metal abundance (Wu & Boada 2019) have achieved high accuracy. However, most previous studies were on galaxy classification, and only a few were about galaxy detection. Among the studies on galaxy detection, Wu et al. (2019) and Lao et al. (2021) use an object detection algorithm for classification. Wu et al. (2019) realized the detection of radio sources based on Faster R-CNN. Lao et al. (2021) used the HeTu5 neural network to achieve the detection of CS, CJ, FRI, and FRII sources.

Compared with classification algorithms (Kim & Brunner 2017; Alhassan et al. 2018) that can only achieve classification, target detection algorithms can simultaneously locate and classify galaxies of interest in astronomical images. Target detection includes the localization and classification of targets. Given the limitation in the location capability of classification algorithms, an image usually needs to be manually cropped before classification, that is, the galaxies that need to be classified from the image must be manually cropped out and then input into the neural network built for training. This procedure for massive astronomical data consumes a large amount of time. By contrast, target detection algorithms can automatically calculate the coordinates of the galaxy that we wish to detect and provide the location information (R.A. and decl.) of the detected galaxy. Hence, they can directly detect and classify original astronomical images observed by radio observatories without manually cropping the galaxy images.

The object detection model YOLO based on a deep neural network and proposed by Redmon et al. (2016) has been developed from V1 to V5. YOLOv5 can realize expeditious real-time detection and has demonstrated superior performance in terms of accuracy. Therefore, we established a galaxy detector based on the improved YOLOv5 target detection model to achieve simple, rapid, and accurate detection and identification of FR0, FRI, and FRII RGs. Our improvements to YOLOv5 are mainly for small galaxy targets, and they enhance the precision of small-target detection and the robustness of the model. We verified our model by using a test set and comparing it with the original algorithm model. Our model demonstrated better performance than the comparison model. While ensuring speed, our improved model could achieve high accuracy and robustness in the test set.

In addition, we used astronomical data from multiple sources, including FIRST⁴ radio and SDSS⁵ optical images, to enhance the effect of galaxy detection. According to the

⁴ See <https://third.ucllnl.org/>.

⁵ See <https://dr12.sdss.org/>.

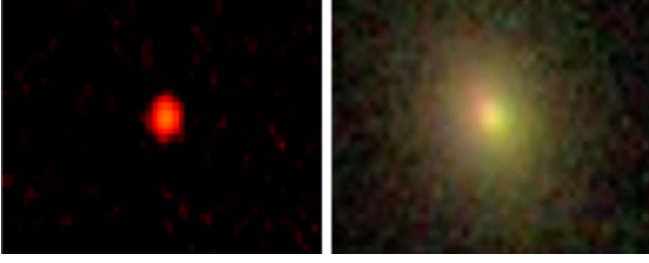


Figure 1. FR0 image sample from FIRST and SDSS.

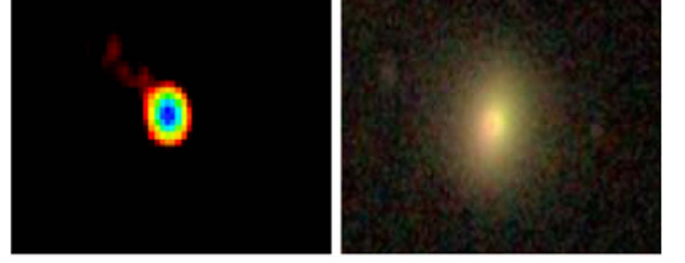


Figure 2. FRI image sample from FIRST and SDSS.

experimental results, the mean average precision (mAP@0.5) of our model reached 89.4%, indicating that it can determine the location and classification of FR0s, FRIs, and FRIIs.

The paper is organized as follows. Section 2 introduces the data set used in this work. Sections 3 and 4 describe the target detection algorithm and our improvements to the model. Section 5 presents the preprocessing and data enhancement procedures, and Section 6 describes our experimental process and experimental environment. Section 7 shows the evaluation of the experimental results. Section 8 presents the discussion of the results, the details and limitations of the experiment, and future work directions. The developed approach is also compared with previous research methods. Section 9 provides the conclusions and summarizes the study.

2. Data

This section describes the composition of the sample. For FR0, FRI, and FRII, we use the FR0CAT (Baldi et al. 2018), FRICAT (Capetti et al. 2017b), and FRIICAT (Capetti et al. 2017a) catalogs, respectively, in which FIRST (Becker et al. 1995), SDSS (York et al. 2000), and NRAO VLA Sky Survey (NVSS) (Hg 1957) data are combined. We construct our radio source samples from three catalogs, each of which contains source location information and their classification labels. Then, we select RGs with relatively obvious features to generate our FR0, FRI, and FRII RG samples.

The FR0CAT catalog is composed of 108 FR0 compact radio source galaxies with a radio source size less than or equal to 5 kpc and the spectral characteristics of low-excitation galaxies, combining the observation results of the SDSS (York et al. 2000), FIRST (Becker et al. 1995), and NVSS (Hg 1957) surveys (Baldi et al. 2018). Sample images of FR0 galaxies in FIRST and SDSS are shown in Figure 1. Compared with FRI, FR0 has a smaller size and higher abundance (Baldi et al. 2018).

The FRICAT catalog is composed of 219 FRIs (Baldi et al. 2018). Sample images of FRI galaxies in FIRST and SDSS are shown in Figure 2. The hosts of FRICAT are all bright ETGs (red early-type galaxies) and classified as LEGs (low excitation galaxies) so they are very uniform. In the 3C sample, the hosts of more powerful FRI galaxies share all of these properties

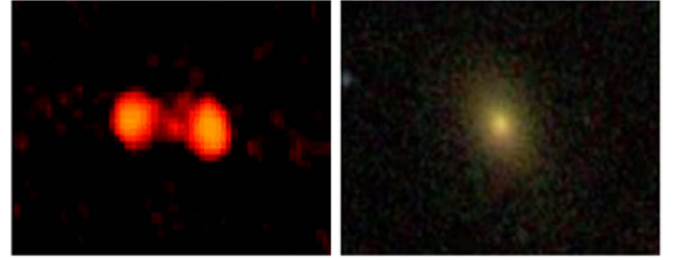


Figure 3. FRII image sample from FIRST and SDSS.

(Capetti et al. 2017a). In terms of color, they are not very different from the general large ETGs (Capetti et al. 2017a). In addition, the FRIs in FRICAT have a radius that extends more than 30 kpc from the host (Baldi et al. 2018).

The FRIICAT catalog is composed of 122 FRII galaxies (Capetti et al. 2017a). Sample images of FIRST and SDSS FRII galaxies are shown in Figure 3. This catalog includes samples obtained by combining observations from SDSS (York et al. 2000), FIRST (Becker et al. 1995), and NVSS (Hg 1957), just like the previous two catalogs. The FRII galaxies in FRIICAT have one or two emission peaks lying in a radius greater than 30 kpc from the center of the main body (Capetti et al. 2017a). At 178 MHz, the brightness difference between FR classes is quite obvious. The dichotomy of FRIs and FRIIs rests with the radio and optical luminosity because on the optical–radio luminosity plane, their separation becomes cleaner (Ledlow & Owen 1996). In addition, FRI RGs are edge-darkened with $R_{\text{FR}} < 0.5$, and FRII RGs are edge-brightened with $R_{\text{FR}} > 0.5$ (Baldi et al. 2018).

3. Target Detection

With the development and extensive application of deep learning, the speed and precision of target detection have gradually improved, and in several aspects, target detection has reached or even exceeded the resolution level of the human eye. Different from the classification algorithm, the target detection algorithm not only realizes the classification of the galaxy of interest in an image but also accurately calculates the coordinates of the galaxy and marks them with a prediction box

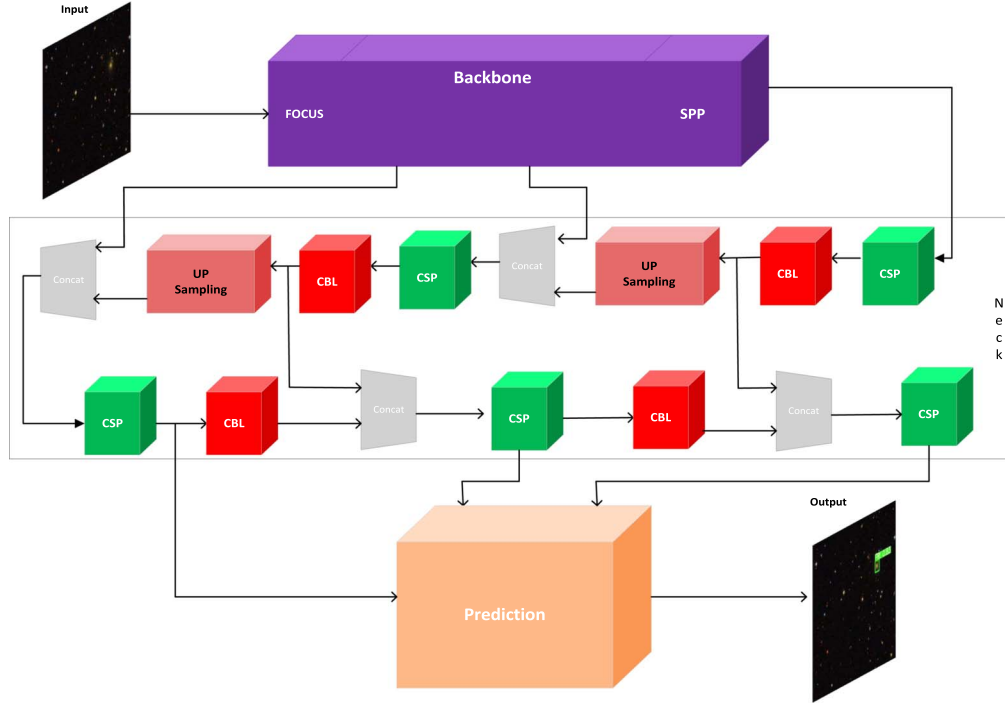


Figure 4. Neural network framework diagram of the original YOLOv5 (Shu et al. 2021). As shown in the figure, YOLOv5 is composed of many modules, and each network module completes one or several corresponding functions, including convolution, pooling, and activation. On the whole, YOLOv5 mainly includes the backbone network and the detection head. The main function of the backbone network is to extract image features and deliver them to the detection head. The detection head is divided into two parts, namely, neck and prediction. The neck layer uses a method similar to FPN+PAN to perform multiscale fusion processing on the features outputted from the backbone network. Then, it sends the results to the prediction layer for classification and bounding box regression.

in the original image so that we can obtain the location information (R.A. and decl.) of the galaxy. That is to say, the detection of galaxies includes the classification and positioning of galaxies.

Widely used target detection algorithms at present include YOLO (Redmon et al. 2016), SSD (Liu et al. 2016), fast R-CNN (Girshick 2015), and faster R-CNN (Ren et al. 2017). After its development from V1 to V5, the YOLO algorithm is now fast and accurate, supports multiscale training, and realizes real-time detection and classification; it is suitable for processing huge amounts of data. YOLO applies the concept of regression to target detection. It is an end-to-end model. We only need to input astronomical pictures into the model; then, it locates and classifies the galaxies of interest in the image at one time and outputs the results. It is convenient and quick. Compared with other algorithms, the YOLO model presents better performance in terms of speed and precision for the galaxy object detection task. Therefore, we select the YOLO algorithm to handle the galaxy object detection task in this work and to serve as the benchmark. YOLO will first locate the galaxy of interest in the input image and frame it with a rectangular box; it will then classify the framed target galaxy to achieve target detection.

The framework of the YOLO (Redmon et al. 2016) algorithm is composed of a convolutional layer and a fully connected layer. The convolutional layer performs feature extraction in the image and combines the functions of the target location and category prediction. Specifically, it uses a combined CNN to obtain the multiscale features of the image and then performs feature fusion through the fully connected network layer in the feature pyramid (FPN) (Lin et al. 2017). Afterward, it transfers the image features to the prediction layer. The prediction layer performs category prediction and bounding box regression based on the image features, calculates the confidence of the category prediction, and generates the target bounding box. Figure 4 shows the architecture of YOLOv5.

Each small square represents a convolution module composed of multiple convolution network structures. With the continuous deepening of the structure, its network feature extraction and feature fusion capabilities have been continuously strengthened, and the capability of deep learning has also been enhanced. The YOLO model (Redmon et al. 2016) calculates the predicted position after the weight is initialized and adjusts the predicted position as the network weight is updated during the training process. During training, the model uses the bounding box to calculate which grid the center of the

object is in, and this grid is responsible for detecting the object (Harishankar & Karthika 2020). In particular, when spanning multiple grids, the object is only detected by the grid containing its center point. In the training phase, the bounding box prediction loss function and the classification-loss functions are used to compare the predicted bounding box with the actual label bounding box and the predicted category with the actual category, calculate the loss, and renew the model. In the prediction phase, YOLO completes the prediction of five attributes (the category of the object in the candidate box (l), the width and height of the candidate box (w , h), and the coordinates of the object center (x , y)) at one time.

Given that the coverage area for small targets, such as galaxies, is small, the resolution is low, the image is blurred, less information is contained, the features (brightness, edge information, etc.) are relatively shallow, and the expressive capability is weak.

To address the problem of performance degradation of the YOLO model when detecting small RG targets, we adopt the following improvement methods: (1) The SE Net (Hu et al. 2018) attention mechanism is used to enhance the neural network's extraction of small-target information features. (2) A set of anchors is added for small targets, and the network structure of FPN (Lin et al. 2017) is adjusted to improve the detection effect. (3) Shallow information is valued, and then the improved FPN+PAN (Wang et al. 2019) is applied to the multiscale fusion of the obtained feature maps. In addition, the background of the radio galaxies is added to assist detection, thereby improving detection accuracy. (4) The initial value of the intersection over union (IOU) (Redmon et al. 2016) is decreased to increase the probability of small targets being detected.

4. Method Used

In astronomical images, the pixels of RGs account for a relatively small proportion. Chen et al. (2016) defined a small target as follows: the relative area of all target instances in the same category, that is, the median of the ratio of the bounding box area to the image area is between 0.08% and 0.58%. According to the relative size definition of the international organization SPIE, a small target is generally smaller than 0.12% of the image, that is, a target smaller than 80 pixels in a 256×256 image is a small target. According to this definition, the RGs we are interested in can be considered small targets in astronomical radio images. The optical image and radio image are basically the same, so this task is a small-target detection task. For small targets, such as galaxies, the coverage area is small, the features (brightness, edge information, etc.) are relatively shallow, and the expression capability is weak. Therefore, neural networks cannot easily extract features, increasing the difficulty of small-target detection and classification. Current improved algorithms for small-target detection

mainly include multiscale learning (Liang et al. 2018), generating superresolution feature representation, presenting attention mechanisms, processing differences in data sets, and introducing context information (Oliva & Torralba 2007). Deriving inspiration from these directions, we propose an improved galaxy object detection model for the classification and detection of galaxy small targets.

We use the attention mechanism (AM). AM is modeled on the visual selection mechanism of the human eye. When we look at objects, we can focus on one object while selectively ignoring other objects. Similarly, AM allows our neural network to focus on the features that are helpful for the classification and positioning of galaxies. With regard to the features that are not important or even unfavorable to model classification, the attention mechanism reduces the learning intensity by reducing its weight. The introduction of AM allows our model to filter the input image features and capture the critical parts during training. We also use the squeeze-and-excitation network (SE Net) (Hu et al. 2018) attention module. The convolution operator allows the deep convolutional neural network to fuse the channel and spatial information in the local receptive field of each layer to extract perfect information features for learning and prediction. It is the most important part of the CNN. SE Net, proposed by Hu et al. (2018), is interested in channel information. SE Net explicitly models the dependencies between channels; it improves the model's sensitivity to channel features, helps fuse complete information features, and enhances the performance of the network. For our galaxy image detection task, SE Net can significantly improve the performance of our model with a small additional computational cost. We introduce SE Net (Hu et al. 2018) in the form of the SELayer module into the network model we constructed to strengthen the extraction of information features. The neural network can analyze and process the channel information from different local receptive fields and give different attention, thereby greatly optimizing our galaxy detection classification and positioning model. Figure 5 shows the basic structure and processing flowchart of SE Net.

Next, we modify the number of anchors (Ren et al. 2017) present in the original YOLOv5 model and add a set of anchors with relatively small values for the detection of galaxy small targets. The training process of YOLO generates many anchors in the image and then continuously reduces the loss function to make the generated anchors constantly approach the real anchor (the anchor where the object we are interested in is). Afterward, the anchor with the best effect produced by the training is selected as the final prediction anchor. As the target area shrinks, the anchor containing the target also decreases, leading to a reduction in the probability of small targets being detected (Wang et al. 2021), as shown in Figure 6. To manage this problem, we increase the probability of a small object being successfully detected by increasing the set of anchors with relatively small values.

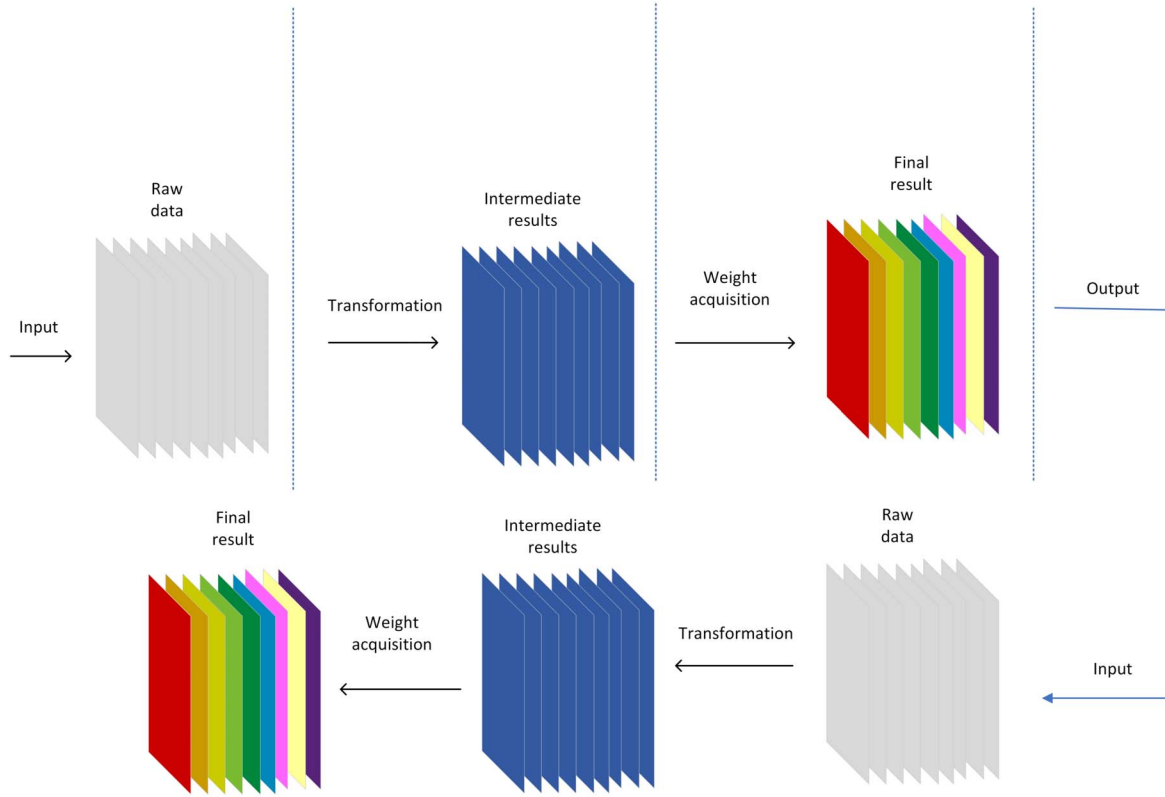


Figure 5. Basic structure and processing flowchart of SE Net. SE Net transforms, compresses, and excites the input raw data to obtain the weights of different channels (scalar between 0 and 1). Then, SE Net uses the obtained weights to weight each channel of the intermediate result and derive a new weighted feature (i.e., feature recalibration). This AM makes the deep neural network focus on channel features that are useful for detection while suppressing useless features (Chen & Fan 2020). Many such modules can be combined into a network, and in this figure, we show the combination of two such modules.

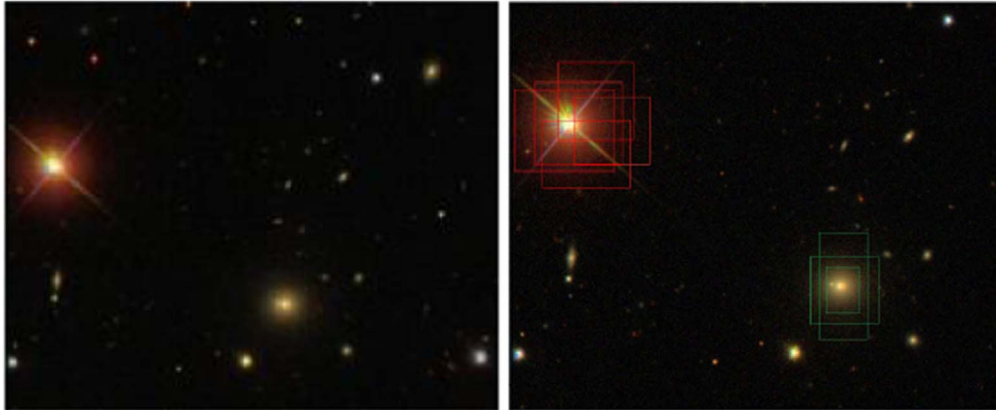


Figure 6. Anchor-matching graph. Assume that we want to detect the large and small galaxies in the image on the left. The image on the right shows that the number of anchors matched by the large target is much larger than that of the small target. The greater the number of matching anchors is, the greater the probability of the target being detected.

The original YOLOv5 has three detection layers, which correspond to three sets of initial anchor values. Compared with conventional targets, small targets have fewer available pixels, and as the number of network layers increases, the

feature information and location information of small targets are gradually lost, making them difficult to be detected by the network. These characteristics cause small targets to require deep semantic information and shallow representation

information. The original YOLOv5 combines and uses FPN (feature pyramid network) (Lin et al. 2017) + PAN (pixel aggregation network) (Wang et al. 2019) for multiscale learning. To improve the detection accuracy of small galaxy targets and apply our added anchor, we improve the structure of FPN (Lin et al. 2017) in the original YOLOv5 model. We add several operational layers to the detection head of YOLOv5, so that after the 17th layer, our model continues to upsample the feature map, thus allowing the feature map to continue to expand. In addition, we fuse the acquired feature map and the second layer feature map in the backbone network with the concat module (a network module for feature fusion) at the 20th layer to obtain a larger feature map for the detection of small galaxy targets. Then, we add a small-target detection layer in the 31st layer, using a total of four layers to detect. Although the increase in detection layers also increases the amount of calculation, which results in a decrease in the model's inference detection speed, it is a good improvement for the detection effect of small galaxy targets.

The deep layer of the neural network model has a large receptive field, which usually produces good results in the detection of large objects. Meanwhile, the shallow layer has abundant information, which is essential for the detection of small objects. Given that our data sets are all small galaxy targets, we moderately reduces the number of neural network modules to obtain abundant shallow information. Although that increases the size of the generated feature map and the memory burden, abundant detailed information can be obtained, thereby increasing the detection accuracy of small targets. Then, we use the improved FPN+PAN (Wang et al. 2019) method to perform multiscale fusion processing on the features outputted from the backbone network, including deep semantic information and shallow representation information. In addition, in order to better classify and locate FR0s, FRI, and FRII, we take the background into consideration and appropriately expand the detection background of FRI to assist detection, which increases the difference between the three, thereby increasing the accuracy of detection,

$$\text{IOU} = \frac{\text{intersection}}{x}. \quad (1)$$

To effectively obtain the features, we appropriately reduce the original IOU (Redmon et al. 2016) threshold setting of the original YOLOv5 model, thereby improving the precision of small-target detection. IOU (Redmon et al. 2016) is used to measure the degree of overlap between the prediction box and the true box, and its calculation is shown in Equation (1). IOU is defined as a measure of the precision of object positioning. Generally, a low IOU threshold (IOUT) reduces the quality of the sample; a high IOUT reduces the number of samples, resulting in an imbalance among the samples, which easily loses the detection frame of small objects (Zhang et al. 2021). However, if the scales of the objects to be predicted do not

differ much, that is, when the scales of most objects in the data set are the same (Zhang et al. 2021), appropriately reducing IOUT can achieve the maximum extraction of small-target features, thereby improving the classification and positioning accuracy for small objects.

5. Image Preprocessing and Data Augmentation

The factors to be considered when selecting samples are the large number of samples, high resolution of images, and freely available images (Aniyan & Thorat 2017). For these reasons, we decided to use FIRST radio and SDSS optical image data, which help locate and classify images accurately. The FIRST survey (Becker et al. 1995) mapped almost a quarter of the sky by detecting a 1.4 GHz source with the sensitivity of $1 \text{ mJy } \text{bm}^{-1}$ and a resolution of $5''$, and it covered the northern and southern areas. The SDSS survey (York et al. 2000) also detected and covered the two areas. In the SDSS survey (York et al. 2000), 3D universe maps were created, with one-third of the sky images. We download the RG image data of FR0, FRI, and FRII; select RGs with relatively obvious features; and then perform data enhancement and preprocessing on the downloaded images.

We first clean the image data from FIRST and SDSS to eliminate noise in astronomical images and make the source we are interested in highly prominent, which to a certain extent can remove the interference of background noise on the model. In addition, to expand our data set, we rotate our image and generate artificial images; that is, for each marked image, we rotate it with randomly generated angles in different angle intervals. Rotation can significantly change the direction of objects without adding topology information. In addition, to avoid holes, we adopt the accurate bicubic interpolation method in the rotation process. In order to improve the detection effect, we moderately increase the size of the real box in the label to increase the difference between FR0, FRI, and FRII RGs. On the one hand, this process expands the data set of our training model and enriches the diversity of the data set. On the other hand, it improves the detection performance of the model and enhances the robustness and generalization capability of our galaxy detection positioning and classification model.

The radio and optical images of FR0, FRI, and FRII RGs are shown in Figures 1–3, respectively. After data enhancement, we obtain 4538 optical images and 4538 radio images. Table 1 shows the number of original radio images and optical images, as well as the number of radio images and optical images after data enhancement. From the data-enhanced images, we select images with prominent radio sources, which contribute to the classification and positioning. Because the number of images in the data set is not large, in order to better train the model, from the selected images, we randomly select 70% of the images in the data set as the training set and 20% of the images as the

Table 1

The Number of Samples in Our Data Set before and after Data Enhancement

Type	Original FIRST Sample	Original SDSS Sample	Data-enhanced FIRST Samples	Data-enhanced SDSS Samples
FR0	108	108	1127	1127
FRI	219	219	2143	2143
FRII	122	122	1268	1268
Total	449	449	4538	4538

validation set, and use the remaining images as the test set. After using the verification set to complete the adjustment and verification of the model hyperparameters, we use the selected enhanced optical and radio data and their labels in the training set and validation set to train our RG object detection model and achieve the classification and positioning of FR0s, FRIs, and FRIIs.

6. Experiment

In accordance with the image data provided by the FIRST and SDSS websites, we save the radio images from FIRST as fits files, save the optical images from SDSS as JPG files, and perform data enhancement and preprocessing on the downloaded images. From the data-enhanced images, we select images with a prominent radio source and divide the selected data set as training set, verification set, and test set. We first use the training set and verification set to adjust and verify the hyperparameters of our model. Because the number of images in the data set is not large, in order to better train the model, after that, we use FIRST and SDSS images in the training set and verification set to train our models and obtain an improved YOLOv5 galaxy target classification and location model based on radio images and an improved YOLOv5 galaxy target classification and location model based on optical images. Then, we analyze and process the prediction results of the two on the test set to obtain accurate positioning and classification results. In addition, when downloading data, on the SDSS website, we enter the specific coordinates of the galaxy to obtain the optical image and fits file of the corresponding galaxy, and the corresponding galaxy is randomly distributed in the image, while on the FIRST website, we enter the specific coordinates of the galaxy to obtain the radio fits file of the corresponding galaxy and the corresponding galaxy is in the center of the image. For localization purposes, we apply a random offset to the galaxies in the downloaded radio image and make them randomly distributed in the image. Therefore, the positions of radio galaxies may be different in the optical and radio images downloaded from the same world coordinates. This is caused by data downloaded by two different

astronomy websites themselves. However, because we train the two models separately and then derive the respective world coordinates from the respective pixel coordinates obtained from the model positioning, for our model, this difference in the distribution of galaxies in the optical and radio images does not make an impact. The process of converting from pixel coordinates to world coordinates is completed by the corresponding optical fits files and radio fits files, respectively. The world coordinates are the same regardless of whether the two pixel coordinates are the same or not.

Figures 7–9 respectively show the processing effect of the model on the input astronomical image and the simple structure of the entire model. In Figures 7 and 8, among the optical images and radio images, we randomly select one image, respectively, to show the processing effect of the model. Figure 10 presents the entire detection flowchart from input to output.

As shown in Figure 10, we first train optical and radio galaxy detection models using radio and optical images, respectively. Each radio galaxy includes its radio image and optical image, which are separately input into two types of galaxy detection models. In addition, the corresponding label information and fits file information of each radio galaxy are also input into the model. The radio and optical images of each radio galaxy and their respective fits files are downloaded separately by entering the coordinates of the radio galaxy. The label information is generated by the corresponding star table, mainly including the coordinate information and category information of the galaxy in the image. During training, the model locates the corresponding galaxy through label information and extracts and learns its features. During testing, the model compares the predicted classification and localization results with the corresponding labels to obtain the effect and accuracy of the test. The fits file information is mainly used to convert the pixel coordinates of the galaxy detected by the model into the corresponding world coordinates (R.A., decl.). We improve the output of the model so that the obtained world coordinates are directly displayed on the upper-right corner of the image.

Because it is the classification and detection of radio galaxies, we first train the radio image classification and positioning model and trust its results more. In addition, according to our observations, FR0s, FRIs, and FRIIs have morphological differences in optical images. Because deep-learning algorithms can capture the feature attributes and differences between different objects in an image, we try to train and test the optical image classification and positioning model that achieves good results. Because the trained model is faced with massive data, we follow the principle of maximizing accuracy. For classification, we adopt the classification results of the radio image classification and positioning model on the left in Figure 10. For positioning, we compare the positioning results of the two with the actual galaxy coordinates. The positioning results of the optical image classification and



Figure 7. Effect display of input and output astronomical images from SDSS.

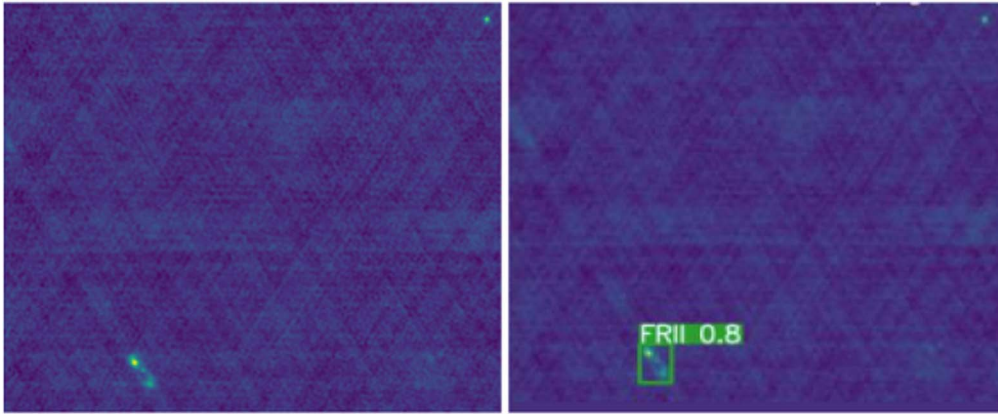


Figure 8. Effect display of input and output astronomical images from FIRST.

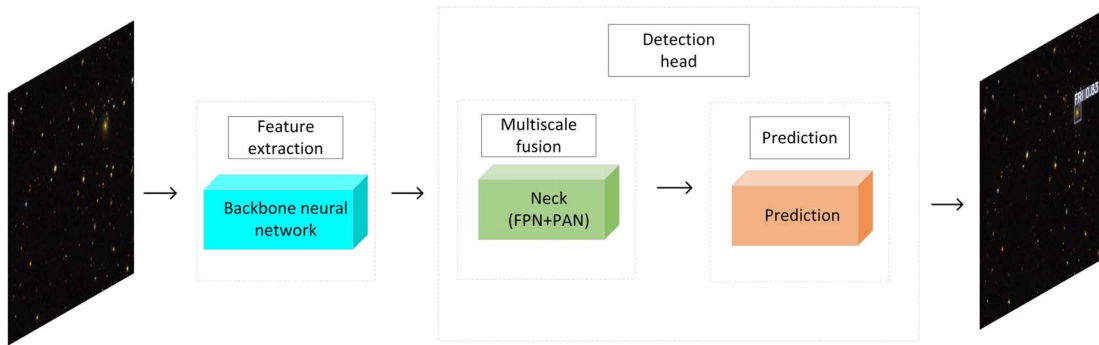


Figure 9. Simple structure of the entire galaxy classification and positioning model. Our improved model marks the detected FR0, FRI, or FR II galaxies in the original image and outputs the position information (R.A., decl.) and classification information of the galaxy.

positioning model on the right in Figure 10 are more accurate, so we mainly adopt its positioning results. The host galaxy position determined from the right column is provided as the location of the radio galaxy observed on the left in Figure 10.

Compared with classification algorithms, object detection algorithms can not only classify objects but also locate objects. Therefore, according to the characteristics of the target detection algorithm, we add the content of locating radio

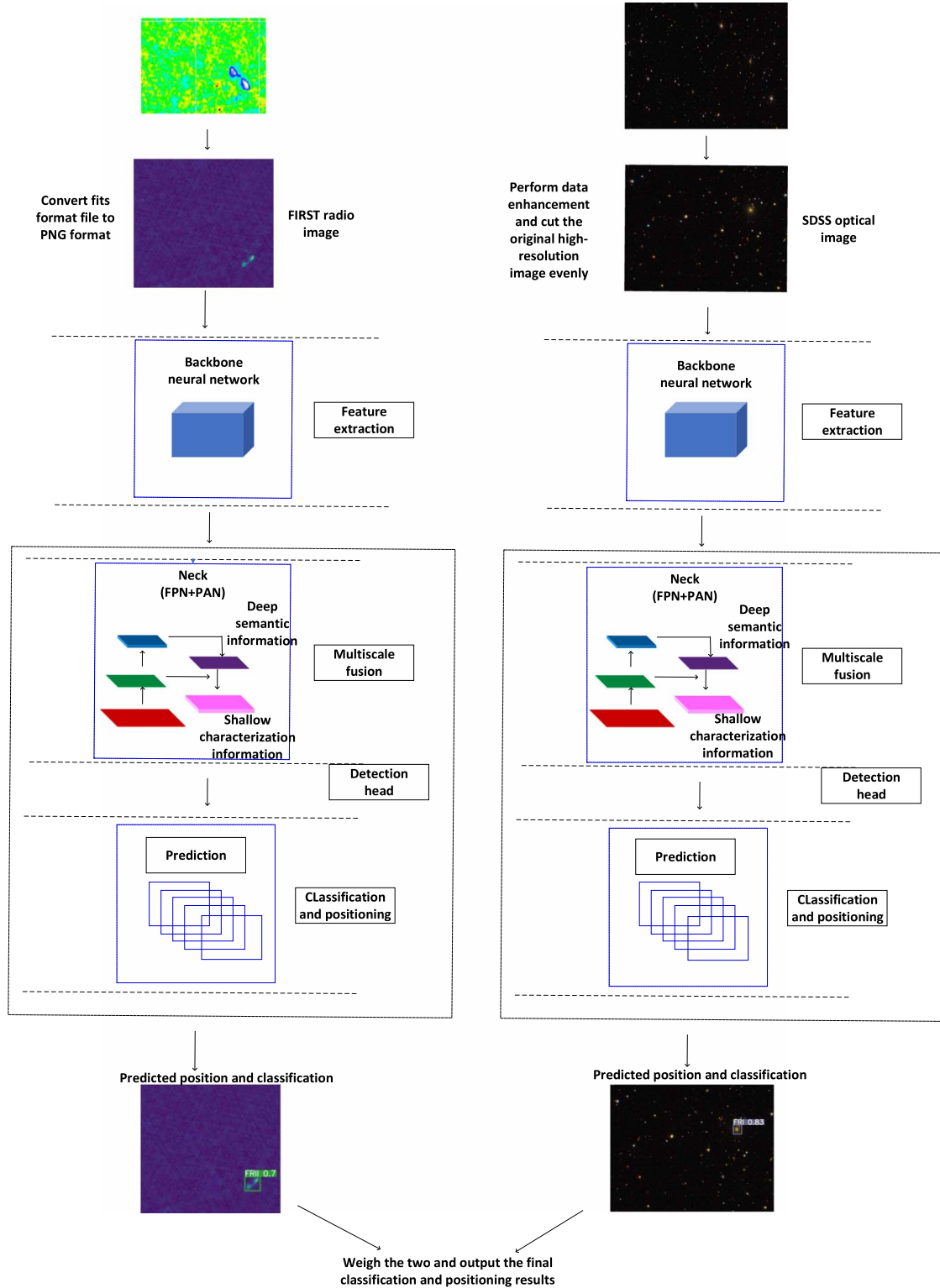


Figure 10. Entire detection flowchart. This picture describes the whole process from the preprocessing of astronomical images to the input and then to the output of the prediction results. The astronomical image input to our improved model first enters the backbone network part. The model extracts detailed image features through the backbone network containing the attention module. Then, the model sends the obtained feature map to the neck part of the detection head, which uses a method similar to FPN+PAN to achieve multiscale fusion of the feature map by downsampling and then upsampling. Afterward, the model sends the feature map fused with deep semantic information and shallow representation information to the prediction part of the detection head and performs regression of the prediction frame and category prediction to obtain the final result.

Table 2
Experimental Hardware and Software Environment

Experimental Environment	
GPU	2080ti
Operating system	Windows 10
Computer language	Python 3.8
Python editor	PyCharm
Function library	Pytorch 1.8.0 CUDA 11.1

galaxies by classifying radio galaxies. Our classification of radio galaxies is the main part, and localization is an extension of the classification. Because the YOLO target detection algorithm can obtain the pixel coordinates of the galaxy and its category, we make full use of the pixel coordinates it outputs plus the world coordinates of the image to determine the world coordinates (R.A., decl.) of the galaxy in the image. Because the two models trained with optical and radio data are performed independently, they do not affect each other. The purpose of models trained with optical images is not to increase the performance of models trained with radio images but to better determine the world coordinates of galaxies from pixel coordinates. As we said earlier, models trained on optical images perform more satisfactorily in this respect than models trained on radio images because the galaxies in optical images are more regular. Therefore, if we input the position coordinate information or the fits file of the astronomical image at the same time we input the astronomical image into the model, we can obtain not only the category of the galaxy but also its world coordinate. The positioning function is an extension based on the classification function, which can simplify our processing of astronomical images and help automate image processing.

Our hardware and software experiment environment is shown in Table 2. Given the huge number of images processed, in terms of hardware, we use NVIDIA’s 2080ti graphics card to speed up the image processing of the model, thereby shortening the training time of the model. We also utilize the new version of Compute Unified Device Architecture (CUDA) 11.1 and the corresponding Pytorch 1.8.0 function library to make full use of the graphics card resources.

7. Model Evaluation and Experimental Results

In this section, we first describe the evaluation indicators of the model. Then, we show the detection performance of our improved galaxy classification and positioning model on FR0, FRI, and FRII radio and optical image data sets, and compared it with the performance of the classification neural network model of Aniyani & Thorat (2017). Finally, we show the actual detection effect of our improved galaxy detection model.

7.1. Evaluation Index

We mainly use mAP (mean average precision), recall, and precision to assess the positioning and classification effects of the improved galaxy detection model.

Precision and recall are two metrics used to evaluate the quality of results. From their definitions, precision is the fraction of relevant instances among all retrieved instances, while recall is the fraction of retrieved instances among all relevant instances. The higher the precision and recall rates are, the better the detection effect of the model is. The calculation of precision and recall and the drawing of the P - R diagram are shown below. If IOU exceeds the specified threshold that guarantees accurate positioning and the probability of the sample exceeds the given threshold that guarantees accurate classification, then the predicted galaxy is considered to be a positive sample of the corresponding galaxy marked in the prediction box. Based on this, we calculate TP, TN, FP, and FN in the model detection results and then using Equations (2) and (3), we can calculate the precision and recall at this time. Considering that different threshold selections correspond to different positive samples, which lead to changes in precision and recall, we connect the (P, R) in the 2D coordinate system corresponding to different thresholds into a smooth curve, which is called the precision–recall curve (P - R curve).

Corresponding to the target detection algorithm, mAP (Everingham et al. 2015), which is the area enclosed by the P - R diagram and the coordinate axis, is the most scientific, convincing, and important evaluation criterion. We use mAP@0.5 and mAP[0.5:0.95] corresponding to the YOLO algorithm to evaluate our model. mAP@0.5 represents the average value of precision predicted by all class labels. The area enclosed by the respective P - R curves and coordinate axes corresponding to FP0, FRI, and FRII RGs is the AP of the corresponding category. We calculate the mean of AP and then derive mAP@0.5 for all classes. In addition, by calculating the mean value when the IOU threshold is 0.5, 0.55, 0.6, 0.65, 0.7, 0.75, 0.8, 0.85, 0.9, and 0.95, we obtain mAP[0.5:0.95]. As another evaluation criterion, mAP[0.5:0.95] is highly sensitive to the position of the detection frame, and our improved model achieves a higher value on this evaluation index than the original YOLOv5. This result shows that our improved model is better at locating the position of the galaxy than the original YOLOv5:

$$\text{precision} = \frac{\text{TP}}{\text{TP} + \text{FP}} \quad (2)$$

$$\text{recall} = \frac{\text{TP}}{\text{TP} + \text{FN}} \quad (3)$$

where for FR0, TP (true positive) indicates that the source is predicted to be an FR0 and it is actually FR0 and IOU exceeds the specified threshold. FP (false positive) indicates that the source is predicted to be an FR0 but it is not actually FR0 or

Table 3Comparison of the Recall (R), Precision (P), and mAP Evaluation Indexes of the Convolutional Neural Network and Our Improved YOLOv5 Model

Means	Recall Rate(%)	Precision Rate(%)	mAP[0.5:0.95](%)	mAP@0.5(%)
CNN of Aniyen and Thorat	91	91(FRI) 75(FRII)		
Our improved YOLOv5	85.5	87.1	43.2	89.4

IOU is below the specified threshold. FN (false negative) indicates that the source is not predicted to be an FR0, but it is actually an FR0 and IOU exceeds the specified threshold.

7.2. Experimental Results and Performance

We compare the performance of our model to the classification model of Aniyen & Thorat (2017). The recall, precision, and mAP of the two models are shown in Table 3. Aniyen & Thorat (2017) use convolutional neural networks to classify FRI, FRII and bent-tailed RGs, which is a representative RG classification network. The model of Aniyen & Thorat (2017) achieves 91% and 75% classification accuracy and 91% classification recall on FRI and FRII RGs, respectively. If we only discuss the performance of the classification, the classification network of Aniyen & Thorat (2017) is better than the object detection model. This is determined by the characteristics of the algorithm itself. The classification algorithm only completes the classification of a complete image, while the YOLOv5 target detection algorithm completes the localization and classification of the target object in the image at the same time. YOLOv5 will first find the object we want to detect from the picture, get its pixel coordinates and frame it, and finally, classify it. In summary, Aniyen & Thorat's (2017) classified convolutional network has better performance characteristics. However, it is limited by its inability to locate galaxies accurately from the images provided, requiring manual cropping of the input image first to ensure that only the target galaxy is included in the image. For such huge amounts of astronomical data that are available, complex data preprocessing such as manual image cropping is generally unacceptable due to its limitations. In contrast, the improved YOLOv5 target detection model can simultaneously locate and classify the target galaxies from the image. It can directly process astronomical raw images, requiring only simple average segmentation without the need for advanced cropping. Thus, the object detection algorithm is an improvement on the classification algorithm. Therefore, the task of the target detection algorithm is more complex than that of the classification algorithm, which may sacrifice some accuracy. Object detection algorithms are more helpful in automatic astronomical image processing in the face of massive astronomical images. The more automated target detection astronomical image processing algorithm is more advantageous in its use. Given the large number of astronomical images

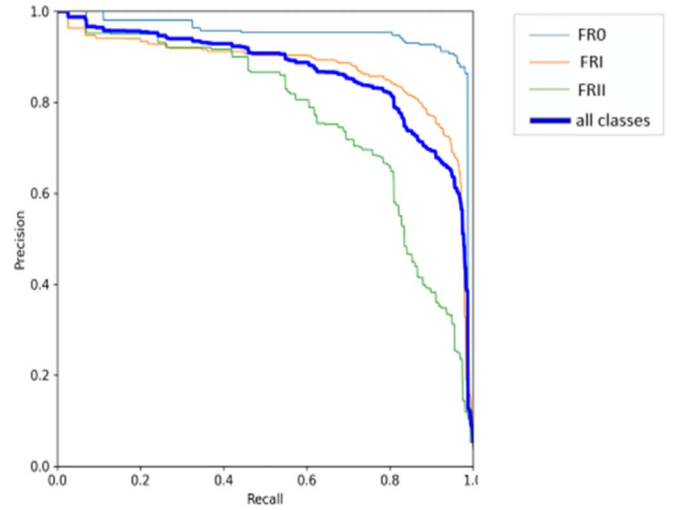


Figure 11. P - R diagrams of our model and the original model. In the P - R diagrams, the horizontal axis measures recall, the vertical axis measures accuracy, and the area enclosed by the coordinate axis and the curve represents mAP, which is the most scientific, credible, and commonly used evaluation criterion for object detection algorithms. The P - R diagrams show the overall P - R curve and the P - R curves of all categories.

available, using the more automated image processing algorithm for target detection is much more beneficial for processing these images in this regard. The target detection algorithm is a more realistic method in order to achieve astronomical image automatic processing. We show the P - R diagram of our model in Figure 11.

One of the reasons the predicted results of YOLOv5 are different from those of Aniyen and Thorat's CNN-predicted classifications is that the features of the predicted source are not obvious and the features are similar to two other kinds of sources. The feature extraction is different because the network structure of YOLOv5 and Aniyen and Thorat's CNN is different. Among the radio sources we selected, the characteristics of some sources are not as obvious and could be confused with the other two types of characteristics, which are especially obvious in FRII sources. The degradation in detection performance of FRII sources has an impact on the overall detection performance. To further illustrate this, we can show the cases where the predicted results are different from the ground truth in Table 5.

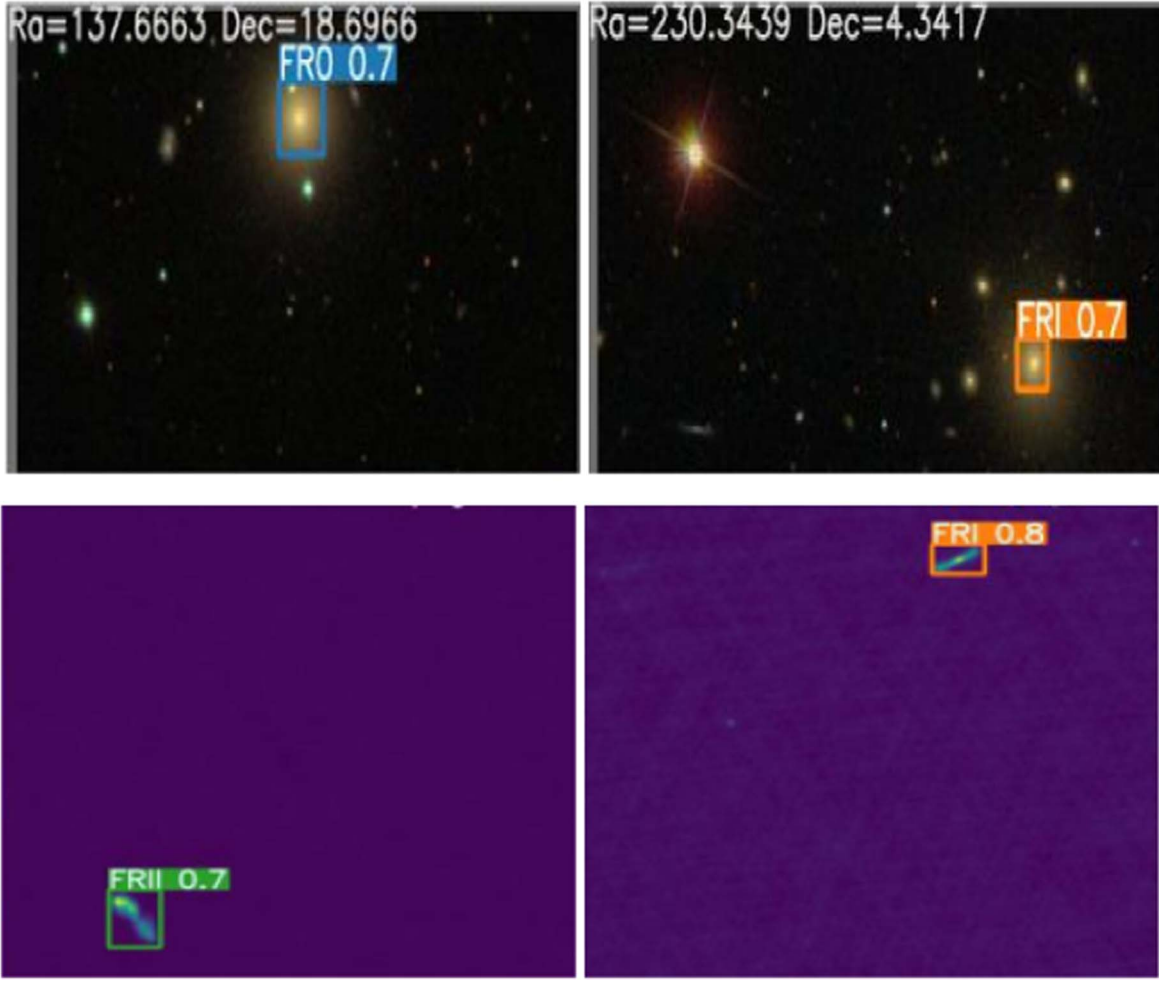


Figure 12. Predicted images from FIRST and SDSS. After training, our galaxy detection model can calculate the coordinates (w, h, x, y) and category (l) of the target in the images and can then create a prediction box to complete the positioning and classification. Above the detection frame is the category and credence of this galaxy (0 1). The upper-left corner of the image gives the location coordinates (R.A., decl.) of the galaxy predicted by the model.

7.3. Experimental Results and Effects

Our improved model can frame the galaxy of interest in the image and give its category. In addition, we improve the output of the optical image training model to convert the pixel coordinates of the galaxy obtained by the model into the actual position coordinates (R.A., decl.) and mark it in the upper-left corner of the image, as shown in Figure 12. Figures 13–15 show the positioning and classification effects of RGs in optical and radio images, respectively.

As shown in Table 4, to further assess the accuracy of the improved galaxy classification and positioning model, we use the improved target detection model to predict the location (R.A., decl.) and category of RGs in randomly selected FR0, FRI, and FRII galaxy image samples and compare the prediction results with the ground truth (exact location information in reality and accurate classification label). The results reveal that

our model has good performance in galaxy classification and position prediction. We can use it to process images generated by sky survey telescopes in the field of astronomy. In addition, for a more comprehensive presentation, we show the cases where the predicted results differ from the ground truth in Table 5.

8. Discussion

The experimental results show that our improved galaxy classification and positioning model based on multisource data can effectively classify and locate FR0, FRI, and FRII RGs in the images. Our model frames the target galaxy in the original image and outputs the location information (R.A., decl.) of the galaxy and the confidence of its category. When faced with massive astronomical image data, in comparison with the speed and accuracy of manual processing, our model can complete



Figure 13. Ground truth of the image samples from SDSS. Based on the location coordinates and category information of the galaxy we are interested in, our model creates a real box to frame the target. Above the real box is the category of this galaxy, and in the upper-left corner of the image are the actual position coordinates of the galaxy.



Figure 14. Predicted image samples from SDSS.

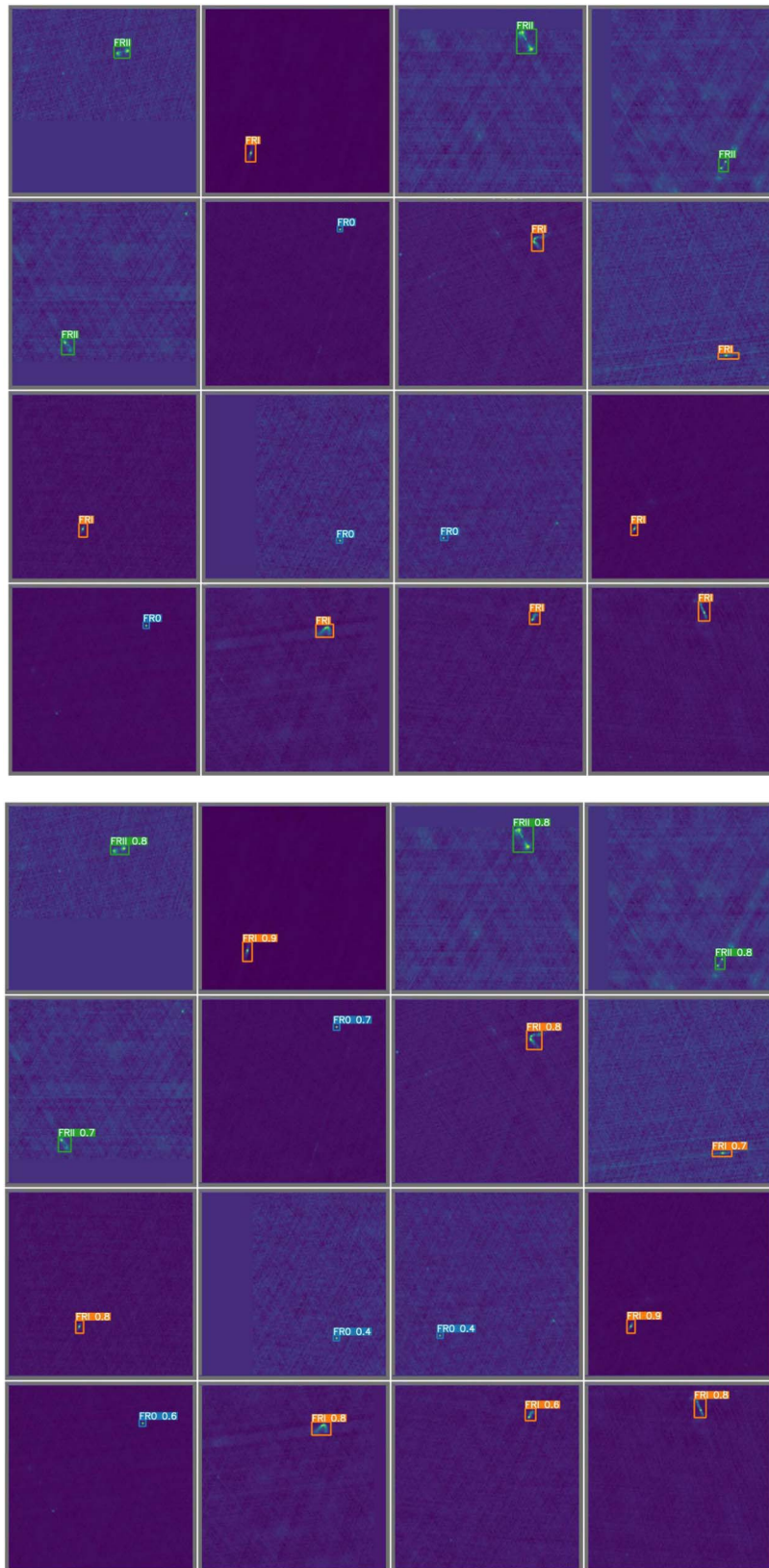


Figure 15. Ground truth of the image samples and predicted image samples from FIRST.

Table 4

Comparison of the Improved Galaxy Classification and Positioning Model Prediction with the Ground Truth of a Few Samples from FIRST and SDSS

















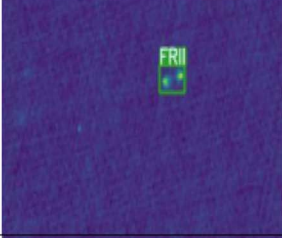
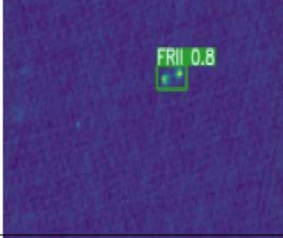


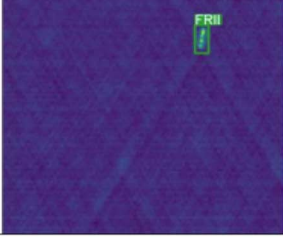
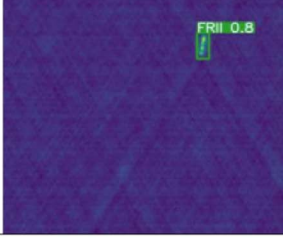

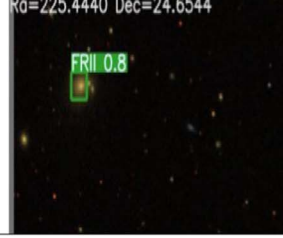
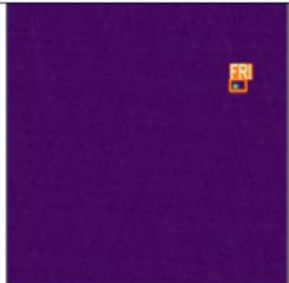
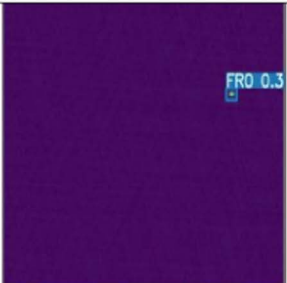


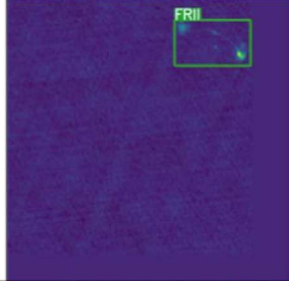
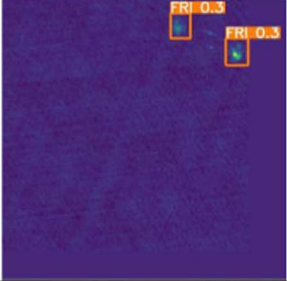
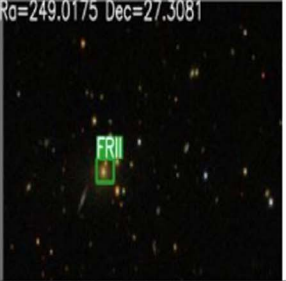

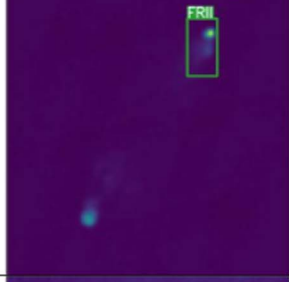
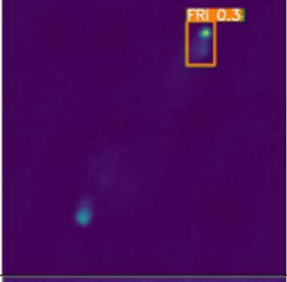



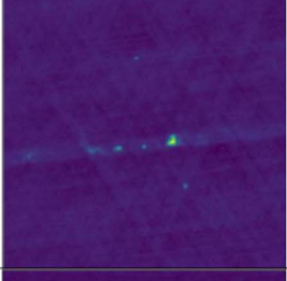
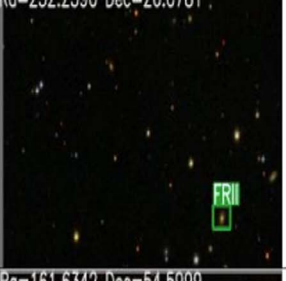

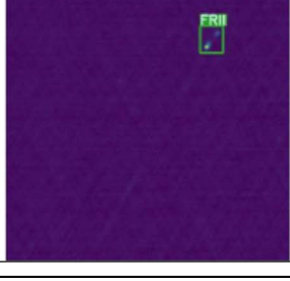
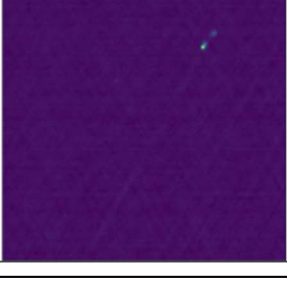
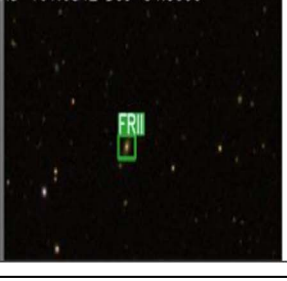
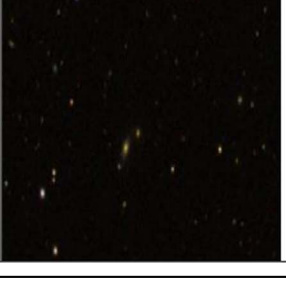
Ground truth image (FIRST)	Predicted image (FIRST)	Ground truth image (SDSS)	Predicted image (SDSS)
			
			
			
			
			
			

Table 5
Cases where the Predicted Results Differ from the Ground Truth

Ground truth image (FIRST)	Predicted image (FIRST)	Ground truth image (SDSS)	Predicted image (SDSS)
			
			
			
			
			

the classification and positioning of FR0s, FRIs, and FRIIs in a short period of time and with relatively high accuracy, which is crucial in making full use of the observation data from large survey telescopes.

Considering the huge amount of astronomical image data, we select the fastest and very mature YOLOv5 target detection algorithm at present to realize the classification and positioning of astronomical images. To deal with the problem of reduced accuracy of deep-learning algorithms when faced with small targets, such as galaxies, in accordance with the characteristics of galaxy images, we improve the YOLOv5 target detection model by adding detection anchors, adjusting the network structure, adding AMs, switching to suitable loss functions, and using data enhancement methods. These modifications improve the adaptability and effect of the model on FR0, FRI, and FRII RG detection tasks. In addition, to improve the positioning and classification accuracy of the model and increase the confidence and accuracy of the detection results, we use FIRST radio image data and SDSS optical image data.

Given the limitations of supervised learning, when the aim is to classify and locate other types of galaxies, image data of the corresponding galaxies must be recollected to train the model. In addition, because the majority of deep-learning algorithms exhibit decreased accuracy when facing small targets, our model still needs further improvement to cope with such decrease in accuracy.

The YOLO target detection model can locate and classify all the galaxies in the image to complete the detection of all galaxies in the image. However, because each of the radio or optical astronomical images we download contains only one radio galaxy, our model only tests the case of one radio galaxy in the image. In our future work, we will further study the scenarios of multiple radio galaxies in the image. In addition, we will improve our method by further improving the loss function and neural network structure to increase the classification and positioning performance of our model for small RG objects. We will also consider the background of the RG in the astronomical image to extract abundantly available features, thereby increasing the performance of the model. In addition, we will expand different types of astronomical galaxies and increase the amount of our data. Thus, our model will be able to locate, detect, and classify other kinds of galaxies, such as compact and BENT galaxies. We will also further expand our work. For example, we can combine other observational galaxy data (e.g., spectral data) with the image data of the galaxy of interest for analysis, which will further facilitate the research of astronomers and improve the accuracy of the model and the reliability of judgment. We will also take into account the cross-matching of data from different sky telescopes when processing astronomical data and fuse the features of different data to increase the accuracy of our model. Another interesting direction for improvement is making full use of the real-time target detection function of YOLOv5 to

realize real-time classification and positioning of galaxies on image data generated by survey telescopes. We will also consider how to better utilize the localization properties of our model in astronomical image recognition.

9. Conclusions

Using the original YOLOv5 model framework, this study proposes an improved galaxy classification and positioning model. In accordance with the characteristics of galaxy images, we improve the YOLOv5 target detection model by adding detection anchors, adjusting the network structure, adding AMs, switching to suitable loss functions, and using data enhancement methods. These modifications improve the adaptability and effect of the model on FR0, FRI, and FRII RG detection missions. The developed model is useful for discovering and locating the location of RGs, understanding their formation and evolution law, and studying their attribute characteristics, such as their composition, internal structure, and physical properties.

The improvements and innovations in many aspects of FR0, FRI, and FRII RG detection enabled our model to achieve better performance than the original YOLOv5 model. We use precision, recall, and map@0.5 as evaluation indicators. As evidenced by experiments, our improved model has high performance for these indicators in galaxy detection, proving once again the precision and robustness of the established model. The model can be applied to the classification and positioning of FR0, FRI, and FRII RGs observed by astronomical telescopes.

We are grateful to the anonymous referee, who made valuable suggestions to help improve the paper. This paper was supported by the Shandong Provincial Natural Science Foundation (ZR2020MA064) and the National Natural Science Foundation of China under grant Nos. 11873066 and 12133001, the science research grants from the China Manned Space Project with Nos. CMS-CSST-2021-A04 and CMS-CSST-2021-A06. Funding for the Sloan Digital Sky Survey IV has been provided by the Alfred P. Sloan Foundation, the US Department of Energy Office of Science, and the Participating Institutions. SDSS acknowledges support and resources from the Center for High-Performance Computing at the University of Utah. The SDSS website is www.sdss.org. This research has also made use of images obtained from FIRST. We acknowledge the use of data from FIRST and SDSS.

Data Availability

The data underlying this article are available in FIRST, at <https://third.ucllnl.org/> and in SDSS, at [https://dr12.sdss.org/\(catalog data\)](https://dr12.sdss.org/(catalog data)).

ORCID iDs

Zhen Zhang  <https://orcid.org/0000-0002-3403-8002>

References

- Alhassan, W., Taylor, A., & Vaccari, M. 2018, *MNRAS*, **480**, 2085
- Aniyan, A., & Thorat, K. 2017, *ApJS*, **230**, 20
- Baldi, R., Capetti, A., & Massaro, F. 2018, *A&A*, **609**, A1
- Baldi, R. D., Capetti, A., & Giovannini, G. 2015, *A&A*, **576**, A38
- Becker, R. H., White, R. L., & Helfand, D. J. 1995, *ApJ*, **450**, 559
- Bourke, T., Braun, R., Fender, R., et al. 2015, Advancing Astrophysics with the Square Kilometre Array (AASKA14) in Proc. Sci. Giardini (ITA), 174
- Capetti, A., Massaro, F., & Baldi, R. 2017a, *A&A*, **601**, A81
- Capetti, A., Massaro, F., & Baldi, R. D. 2017b, *A&A*, **598**, A49
- Chen, W., & Fan, B. 2020, in 2020 Chinese Automation Congress (CAC), Shanghai (IEEE), 2821
- Chen, C., Liu, M.-Y., Tuzel, O., & Xiao, J. 2016, in Asian Conf. on Computer Vision (Berlin: Springer), 214
- Everingham, M., Eslami, S. A., Van Gool, L., et al. 2015, *Int. J. Comput. Vision*, **111**, 98
- Fanaroff, B. L., & Riley, J. M. 1974, *MNRAS*, **167**, 31P
- Girshick, R. 2015, (Piscataway, NJ: IEEE) [Google Scholar]
- Hg, W. 1957, *AIP*, **126**, 68
- Harishankar, V., & Karthika, R. 2020, in 2020 5th Int. Conf. on Communication and Electronics Systems (ICCES) (Piscataway, NJ: IEEE), 855
- Helfand, D. J., White, R. L., & Becker, R. H. 2015, *ApJ*, **801**, 26
- Hoyle, B. 2016, *A&C*, **16**, 34
- Hu, J., Shen, L., & Sun, G. 2018, in Proc. IEEE Conf. on Computer Vision and Pattern Recognition (Piscataway, NJ: IEEE), 7132
- Jarrett, T. H., Masci, F., Tsai, C., Petty, S., & Benford, D. 2011, American Astronomical Society Meeting Abstracts, 218, 328
- Johnston, S., et al. 2008, *ExA*, **22**, 151
- Jonas, J. & Team MeerKAT 2016, MeerKAT Science: On the Pathway to the SKA, 1
- Kim, E. J., & Brunner, R. J. 2017, *MNRAS*, **464**, 4463
- Lao, B., An, T., Wang, A., et al. 2021, *Sci. Bu.*, **66**, 2145
- Ledlow, M. J., & Owen, F. N. 1996, arXiv:astro-ph/9607014
- Liang, Z., Shao, J., Zhang, D., & Gao, L. 2018, in Pacific Rim Conf. on Multimedia (Berlin: Springer), 554
- Lin, T.-Y., Dollár, P., Girshick, R., et al. 2017, in Proc. IEEE Conference on Computer Vision and Pattern Recognition (Piscataway, NJ: IEEE), 2117
- Liu, W., Anguelov, D., Erhan, D., et al. 2016, in European Conf. on Computer Vision (Berlin: Springer), 21
- Maslej-Krešňáková, V., El Bouchefry, K., & Butka, P. 2021, *MNRAS*, **505**, 1464
- Oliva, A., & Torralba, A. 2007, *Trends in Cognitive Sciences*, **11**, 520
- Redmon, J., Divvala, S., Girshick, R., & Farhadi, A. 2016, in Proc. IEEE Conf. on Computer Vision and Pattern Recognition (Piscataway, NJ: IEEE), 779
- Ren, S., He, K., Girshick, R., & Sun, J. 2017, *ITPAM*, **39**, 1137
- Shu, L., Zhang, Z., & Lei, B. 2021, *Opt. Optoelectron. Technol.*, **19**, 69
- Wang, W., Xie, E., Song, X., et al. 2019, in Proc. IEEE/CVF Int. Conf. on Computer Vision (Piscataway, NJ: IEEE), 8440
- Wang, Z.-Z., Xie, K., Zhang, X.-Y., et al. 2021, *IEEE Access*, **9**, 56416
- Wu, C., Wong, O. I., Rundick, L., et al. 2019, *MNRAS*, **482**, 1211
- Wu, J. F., & Boada, S. 2019, *MNRAS*, **484**, 4683
- York, D. G., Adelman, J., Anderson, J. E., et al. 2000, *AJ*, **120**, 1579
- Zhang, J., Meng, Y., & Chen, Z. 2021, *IEEE Access*, **9**, 96559